Int. J. Electrochem. Sci., 6 **(2011)** 6718 - 6732

International Journal of
ELECTROCHEMICAL
SCIENCE
www.electrochemsci.org

Effect of Various Heat Treatment Conditions on Microstructure, Mechanical Properties and Corrosion Behavior of Ni Base Superalloys

N. El-Bagoury[1,2], *Mohammed A. Amin*[1,3,*], *Q. Mohsen*[1]

[1] Materials and Corrosion Lab (MCL), Chemistry Department, Faculty of Science, Taif University, P.O. Box 888, Haweiyah, Saudi Arabia.
[2] Casting Technology Lab., Manufacturing Technology Dept., Central Metallurgical Research and Development Institute, CMRDI, P. O. Box 87 Helwan, Cairo, Egypt.
[3] Chemistry Department, Faculty of Science, Ain Shams University, P.O. Box 11566, Abbassia, Cairo, Egypt.
[*]E-mail: maaismail@yahoo.com

Received: 5 October 2011 / *Accepted:* 11 November 2011 / *Published:* 1 December 2011

The effect of heat treatments on the microstructure and mechanical properties of Ni base superalloys was investigated. The tested alloys were manufactured by investment casting under various conditions of superheat. These alloys were solution treated at 1120 and 1180 °C for 2 h followed by air cooling before aging process at 845 °C for 24 h. The volume fraction, V_f, of TCP (Tetragonal Close Packed) phases decreases as the solution treatment temperature increases. The grain size of aged specimens treated at 1180 °C was found to be coarser than that treated at 1120 °C. The V_f of primary γ' particles in aged alloys treated at 1120 °C was higher than that of alloys treated at 1180° C. However, V_f of secondary γ' precipitates in aged alloys treated at 1180 °C was found to be larger than that in alloys treated at 1120 °C. Hardness values of aged alloys treated at 1120 °C were lower than those measured for 1180 °C treated alloys. The effect of solution heat treatments on the corrosion behavior of the tested Ni base superalloys was also studied via monitoring corrosion rates of these alloys in 1.0 M H_2SO_4 solution at 25 ^oC. Rates of corrosion were monitored based on ICP-AES (inductively coupled plasma atomic emission spectrometry) method of chemical analysis via determination of Ni^{2+} in solution after each corrosion test. The amount of nickel released into the corrosive medium was taken as a measure of the corrosion rate. The corroded surfaces were examined by the light microscope. Results obtained revealed that the corrosion rate of the aged alloys treated at 1120 °C was much higher than that of aged alloys treated at 1180 ^oC. At the same temperature, alloys with fine microstructure were found to resist corrosion compared to those with coarse microstructure. The electrochemical behavior of such alloys was also studied in 1.0 M H_2SO_4 solution based on polarization measurements. The four tested Ni alloys exhibited a passive behavior in 1.0 M H_2SO_4 solution, and their anodic behavior in the active dissolution region was discussed.

Keywords: Ni base superalloys; Heat treatment; Microstructure; SEM, Corrosion; Sulphuric acid; Monitoring corrosion rates; Tafel extrapolation method

1. INTRODUCTION

Nickel-base superalloys have been widely used, because of the high volume fraction of γ' phase and better high temperature properties, to make the blade parts of the aero-engine [1–5]. As the microstructure plays an important role in the mechanical properties of the alloys, therefore it is worth to study effects of the microstructure closely. There is considerable interest in heat treatment processes of improving the alloy properties [6-8].

Heat treatments are usually recommended for nickel-base superalloys and suggested primarily to produce high volume fraction and better size distribution of γ' precipitates, which give an optimum stress rupture property [9,10].

The strengthening of nickel-based superalloys is mainly obtained by the coherent precipitation of a large amount of Ni_3Al type γ' % phase in a nickel-based γ matrix. The morphology of the γ' % precipitates in these alloys has been well documented and a large variety of the γ' % precipitate shapes has been observed (spheres, cubes, aligned cubes, plates, short plates, doublet of short plates, octet of cubes, large plates, rafts,…) [11- 14].

The heat treatments usually recommended for nickel-base superalloys are suggested primarily to produce high volume fraction and better size distribution of γ' precipitates which give optimum stress rupture property. In as-cast alloys with a high volume fraction of γ/ γ' eutectic, the complete dissolution of γ' by the appropriate heat treatment is of extreme importance [15]. The high melting temperature of Ni base superalloys frequently allows for refinement of the γ' microstructure with a solution heat treatment followed by one or more steps of ageing heat treatments. Both γ' precipitate size and volume fraction (V_f) can significantly influence the mechanical properties of the single crystal nickel-base superalloys at room and elevated temperature [16].

Nickel-base alloys are vitally important to modern industry due to their ability to withstand a wide variety of severe operating conditions involving corrosive environments, high temperatures, high stresses, and combinations of these factors [17]. Ni-base alloys possess excellent corrosion resistance, which is the important property demanded in the nuclear industry. The excellent corrosion resistance is largely due to the Ni-base alloys surfaces protected in aqueous electrolytes or moist air by ultrathin dense oxide/hydroxide films. The films act as an effective barrier to separate the substrate alloys from the corrosive environment and thus protects the substrate alloys from further corrosion processes [18-20]. Therefore, nickel-base alloys exhibit unusual corrosion resistance property in many corrosive environments.

Unfortunately, the passive film does not afford complete protection of the substrate alloys. For instance, in tribocorrosion systems, tribological contact can often damage or even remove the passive film, as a result, exposing the active substrate alloy surface to the corrosive environment, resulting in an anodic dissolution of the alloys. In addition, certain aggressive ions (e.g., Cl^-, Br^-) can also induce passivity breakdown, resulting in various forms of localized corrosion, such as pitting attack and stress corrosion cracking [21-24]. Localized corrosion processes can result in the rapid penetration of a

cavity pit or crack into the alloy substrate, thus leading to premature failure. Acid media can also result in corrosion attack.

Considering the potential applications of Ni-base superalloys, studying the corrosion behavior of such materials is an important parameter for investigation, particularly the generalized corrosion attack occurring in acid media, due to the aggressive environments where these alloys are used. Furthermore, the literature contains very few studies about the corrosion behavior, corrosion rate, and anodic behavior in acid media of these materials. The objective of the present work is two folds; (i) studying the influence of the heat treatment processes on the microstructure of Ni base superalloys produced under different levels of casting superheat. TCP phases and precipitation of γ' particles that affect the mechanical properties and corrosion resistance of alloys were discussed, (ii) monitoring the corrosion rates of the four tested Ni alloys in 1.0 M H_2SO_4 solution, based on ICP-AES method of chemical analysis.

It was also the purpose of the corrosion section of this work to investigate the corrosion and electrochemical behaviour of the tested Ni alloys in 1.0 M H_2SO_4 solution through potentiodynamic polarization technique. Some optical microscope examinations of the corroded surfaces were also performed. The obtained chemical and electrochemical corrosion parameters were discussed on the basis of microstructure studies of the tested alloys, including morphology and volume fraction of different phases.

2. EXPERIMENTAL PROCEDURES

The chemical composition of the investigated Ni base superalloys in this study is shown in Table 1. These alloys were melted under vacuum atmosphere before casting under various casting superheat levels. Low (F) and high (C) superheat levels were applied into two castings. These Ni base superalloys were solution treated at different conditions of 1120 and 1180 ºC for 2 h followed by air cooling. Further aging heat treatment at 845 ºC for 24 h was accomplished for both solution treated alloys.

Optical emission apparatus, ARL3560OES as well as Ni base software were used to determine the chemical composition of the heat treated alloys.

Characterization for microstructure studies including morphology and volume fraction of different phases was carried out by both Zeiss light optical microscope fitted with Hitachi digital camera and JOEL JSM-5410 Scanning Electron Microscope (SEM). The specimens for microstructure examination were ground and polished according to ASTM standard E3 and E768, then etched with 50 ml HCl + 2 ml H_2O_2 (30%) solution. The microanalysis for different phases in the microstructure was performed using EDS in JEOL JSM5410. The Vickers hardness was measured with Akashi Hardness Tester Machine (Akashi Co. Ltd.) under a load of 60 Kg. The mean value over ten measurements was evaluated.

Table 1. Chemical composition of Ni base superalloy, mass %.

Elements Alloy	C	Cr	Mo	W	Ti	Co	Al	Nb	Ta	Ni
	0.54	16.95	2.45	4.36	5.88	10.48	1.49	0.10	1.86	Bal.
	0.47	16.97	2.39	4.27	5.74	10.37	1.41	0.12	1.93	Bal.

All the chemical and electrochemical tests were performed in 1.0 M H_2SO_4 solution, as the corrosive medium, prepared with analytical grade chemicals and doubly distilled water. The solution was naturally aerated and the temperature was held at 25 ◦C using a temperature control water bath. Cylindrical samples for the electrochemical tests were machined carefully and mounted in polyester resin after the electric contact, with special care taken to prevent the presence of crevices. The exposed area was 1.0 cm^2. Before each run, the samples were wet ground with #600-grit silicon carbide (SiC) paper, washed in distilled water, and immersed in the electrochemical cell. The samples were then subjected to open circuit conditions until a steady state potential was reached. This procedure was accomplished in 30 min and the potential value obtained was considered the corrosion potential (E_{corr}).

A conventional electrochemical cell was used, consisting of a platinum counter electrode and Ag/AgCl reference electrode. A Luggin–Haber capillary was also included in the design. The tip of the Luggin capillary is made very close to the surface of the working electrode to minimize IR drop. The electrochemical cell was connected to a potentiostat; Autolab frequency response analyzer (FRA) coupled to an Autolab Potentiostat/Galvanostat (PGSTAT30) with FRA2 module connected to a personal computer. The potentiodynamic polarization measurements were carried out at a scan rate of 2.0 mV s^{-1}, starting from a cathodic potential of -2.0 V up to an anodic potential of 2.0 V.

For corrosion rates evaluated by ICP-AES method of chemical analysis, the Ni^{2+} ions concentration was determined for each tested Ni alloy in a 1.0 M H_2SO_4 solution after an immersion time of 96 h, according to the ASTM G31–72(2004) standard, using Perkin–Elmer Optima 2100 Dual View inductively coupled plasma atomic emission spectrometry (ICP-AES) instrument connected with AS 93 Plus autosampler. Light microscope images were recorded after each immersion test. To obtain clear and detailed images, a mechanical polishing up to 1μm (mirror finish) was performed before each immersion test.

3. RESULTS AND DISCUSSION

3.1. Solution treated microstructure

Solution treatment was carried out for 2 h at both 1120 and 1180 ºC, followed by air cooling. The solution treatment at 1120º C represents the standard solution treatment, while that at 1180 °C represents the modified solution treatment. SEM and EDS emphasized that the σ nodular and interdendritic γ/γ’ phases found in as cast structure were entirely vanish after solution treatment either at 1120 ºC or 1180 °C **[25]**. After solution treatment with various conditions for all as cast specimens, the interdendritic γ/γ’ phase vanished completely from these microstructures.

Density or V_f as well as morphology and size of γ' precipitates are affected by the solution treatment conditions. The morphology of as cast coarse, primary, cuboidal γ' precipitates starts to dissolute in the matrix after solution treatment processes, as shown in Fig. 1. The V_f of these precipitates in as cast microstructure decreases by solution treatment. Solution treatment with 1120 ºC has higher V_f of primary, coarse, γ' precipitates than solution treatment after 1180 ºC. Coarse γ' particles first coalescence with each other, then dissolve in the matrix with solution treatment.

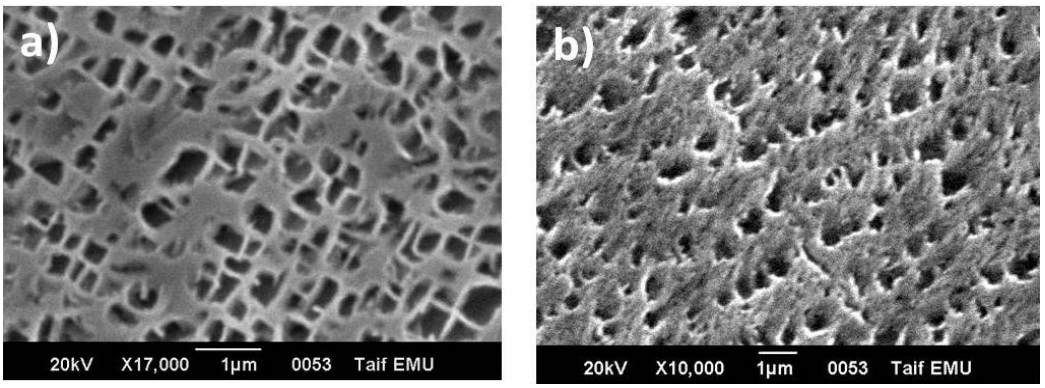

(a) (b)

Figure 1. γ' in as cast **(a)** and **(b)** heat treated microstructures at 1120 °C **[25]**.

The effect of solution treatment temperature on the V_f of TCP phase for different specimens is given in Table 2. Elevating the solution treatment temperature from 1120 to 1180 °C affects significantly the V_f of TCP phase. This V_f decreases by increasing solution temperature from 1120 to 1180 ºC for the same specimen.

Table 2. Effect of solution temperature on V_f of TCP phases [25].

Specimen	V_f at solution treatment Temperature (%)	
F	2.76	1.23
C	4.64	2.36

3.2. Influence of aging on microstructure

The aged microstructures of F and C specimens at 845° C after solution treatment at 1120 and 1180 °C are shown in Figs 2 and 3, respectively. Generally, V_f of TCP phases in interdendritic regions of 1120 °C specimen is higher than that of 1180 °C for both F and C alloys. In other words, high solution temperature dissolves TCP phases such as σ and η phases in the γ matrix. Moreover, casting superheat level has a great effect on V_f of TCP phases. Superheat level has inverse relationship with V_f

of TCP phases; decreasing superheat level increases the TCP phases in interdendritic regions, as it can be seen in Figs. 2 and 3.

The grain size of aged alloys was affected as well by the solution temperature **[26]**. It can be easily recognized that the grain size of F and C alloys with 1180 °C is a little bit coarser than that of 1120 °C for the same conditions, as shown in Fig. 2 and 3.

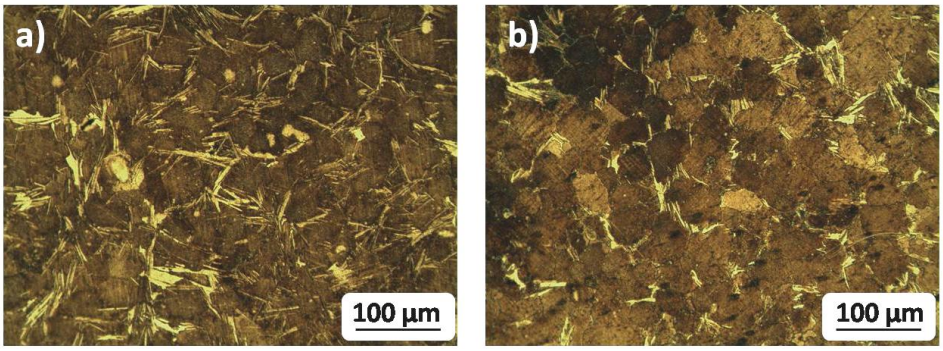

Figure 2. Aged microstructure at 845°C after solution treated at 1120 °C recorded for **(a)** C**, (b)** F**,** alloys.

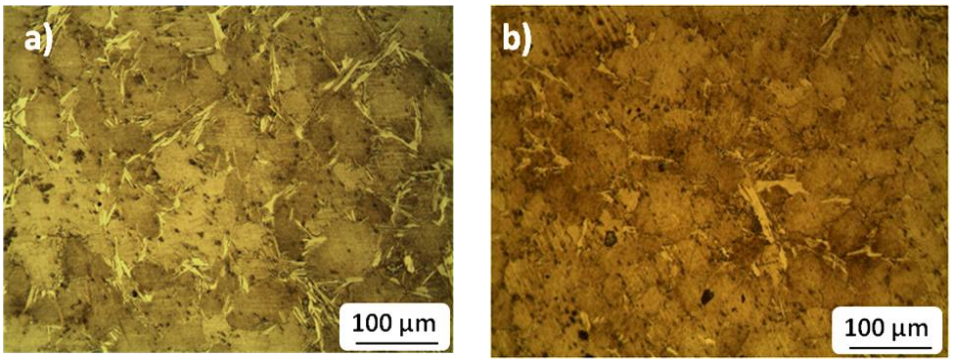

Figure 3. Aged microstructure at 845°C after solution treated at 1180°C recorded for **(a)** C, **(b)** F, alloys.

Figures 4 and 5 show the γ' precipitates in both aged F and C specimens after solution at 1120 and 1180 °C, respectively. It follows from Figs. 4 and 5 that the size of γ' particles in aged C specimen at 845° C for 24 h is coarser than that in F specimen in both cases of solution treatment, 1120 and 1180 °C [25]. The V_f of γ' particles in case of aged F specimen is higher than that in C one after solution treatment at 1120 and 1180 °C. Increasing solution temperature from 1120 to 1180 °C decreases V_f of γ' particles in both F and C specimens. Whereas the solution temperature elevated, the coarse γ' precipitates dissolve in the matrix, lowering the V_f of γ' particles [27].

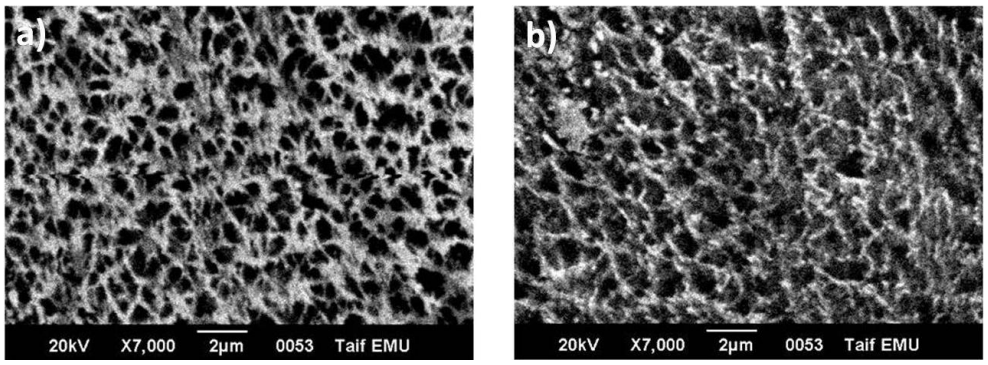

Figure 4. γ' precipitates in specimen with solution temperature at 1120 °C **(a)** F and **(b)** C, after aging at 845 °C.

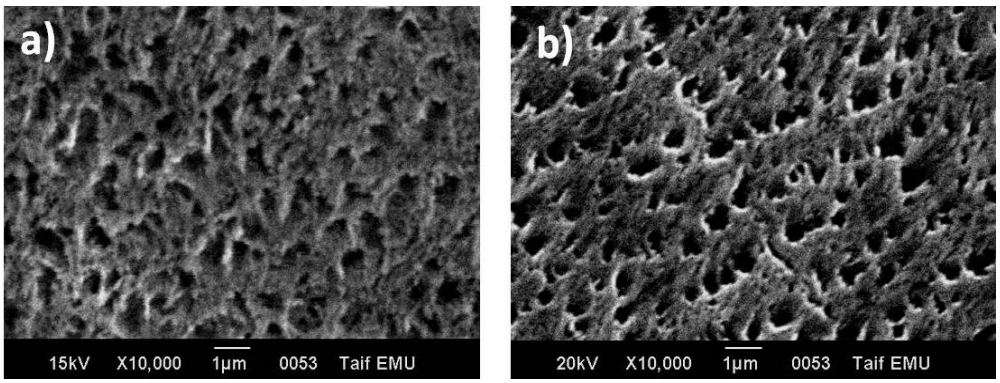

Figure 5. γ' precipitates in specimen with solution temperature at 1180 °C **(a)** F and **(b)** C, after aging at 845 °C.

3.3. Mechanical properties and hardness measurements

Hardness measurements for aged specimens at 845° C for 24 h and solution treated at 1120 and 1180 °C were evaluated, as shown in Table 3. Hardness value has a strong relationship with the γ' characteristics especially volume fraction and size. Moreover, superheat levels affect the hardness values as well. Hardness values recorded for aged F alloys are higher than those of C specimens after solution treatments at both 1120 °C and 1180 °C [28]. In other words, as the superheat level increases the hardness value decreases [29].

Table 3 - Hardness measurements for F and C alloys.

Alloy	1180 °C	1120 °C
F	472	457
C	450	439

Data presented in Table 3 reveal that the hardness values recorded for F and C specimens with 1180 °C are higher than those of 1120 °C. This could be explained on the basis that higher temperature of solution treatment, 1180 °C, has higher effects on the dissolution of coarse γ' in the matrix than in case of 1120 °C. Therefore, V_f of primary, coarse, γ' in case of 1120 °C is higher than that in 1180 °C. However, V_f of secondary, fine, γ' precipitates in 1120 °C is lower than that in 1180 °C. This could be the reason for the higher hardness values recorded for 1180 °C specimens compared with those of 1120 °C ones, see Table 3.

3.4. Corrosion behavior of Ni base alloys in 1.0 M H_2SO_4 solution

3.4.1. Monitoring corrosion rates by ICP method of chemical analysis

It is well known that the electrochemistry of corroding metals involves two or more half-cell reactions. The kinetics of the anodic dissolution of Ni in acid solutions involves uniform dissolution with the reaction path [30]:

$$Ni + H_2O \leftrightarrow NiOH + H^+ + e^- \quad (1)$$

$$NiOH + H^+ \leftrightarrow Ni^+ + H_2O \quad (2)$$

$$Ni^+ \leftrightarrow Ni^{2+} + e^- \quad (3)$$

which considers the water adsorption process in the mechanism of electrooxidation. On the negative side, the H_3O^+ reduction (reaction 4) is the main reaction occurring on the electrode surface.

$$2H_3O^+ + 2e^- \leftrightarrow 2H_2O + H_2 \quad (4)$$

The overall chemical reaction is the sum of the two half-cell reactions (3) and (4):

$$2Ni^+ + 2H_3O^+ \leftrightarrow 2Ni^{2+} + 2H_2O + H_2 \quad (5)$$

Based on the overall chemical reaction presented in Eq. (5), four ways may be suggested to determine the corrosion rate by a suitable chemical method, such as ICP-AES method of chemical, which will be employed here. These are (i) to determine the quantity of Ni lost due to corrosion by weight loss measurements, (ii) to measure the concentration of Ni^{2+} ions which are produced in the test solution as a result of chemical corrosion, based on the cited ICP method of chemical analysis, (iii) to determine the quantity of hydrogen gas which is produced by the corrosion reaction, and (iv) to determine pH changes in solution caused by the consumption of H_3O^+ ions. These four ways for monitoring corrosion rate are well discussed in a previous publication by E. McCafferty [31].

In ICP measurements, known aliquots of the solution containing dissolved Ni^{2+} were withdrawn for each sample after 96 h of immersion in 1.0 M H_2SO_4 solution and analyzed. The

corrosion rate (CR) values recorded for the four samples are expressed as mg cm^{-2} h^{-1} (i.e., mass, in mg, of Ni dissolved as Ni^{2+} per unit area per unit time). The numerical values of corrosion rates were converted into the corresponding corrosion current density (j_{corr}) values using Faraday's law, and subsequently converted into corrosion rates (in mpy) (milli-inches/year; the penetration rate of corrosion through a metal), using Eq. (6) [32]:

$$CR\ (mpy) = (1.288 \times 10^5) \times \{(j_{corr})(E_w) / (d)(A)\} \quad (6)$$

Where j_{corr} is the corrosion current density in (A cm^{-2}), E_W is the equivalent weight in grams/equivalent, d is the density (in grams/cm^3), and A is the sample area in cm^2. For the tested Ni-base super alloy, E_w = 25.41 g/equiv. [32] and d = 8.17 g cm^{-3} (see Practice G1 for density values for many metals and alloys used in corrosion testing). The calculated corrosion rate values (Table 4) were found to be 522, 95, 36 and 21.5 mpy for 1120 C, 1120 F, 1180 C and 1180 F, respectively.

Table 4. Electrochemical parameters and rates of corrosion (associated with polarization measurements) and corrosion rates evaluated from the ICP-AES method of chemical analysis for the four tested Ni-base alloys in 1.0 M H_2SO_4 solution at 25 ^oC.

Tested alloy	j_{corr} / A cm^{-2}	E_{corr} / V	β_c / V dec^{-1}	$(CR)_{Tafel}$ mpy	j_c / A cm^{-2}	j_{pass} / A cm^{-2}	E_{pp} / V	$(CR)_{ICP}$ mpy
1120 C	1.4×10^{-3}	-0.217	-0.22	561	0.02	0.0028	0.204	522
1120 F	2.24×10^{-4}	-0.216	-0.174	89.7	0.017	0.0015	0.193	95
1180 C	8.15×10^{-5}	-0.213	-0.188	32.65	0.0035	0.0003	0.191	36
1180 F	6.17×10^{-5}	-0.209	-0.20	24.72	0.00033	0.00006	0.137	21.5

These findings reveal that the rates of corrosion of F and C specimens with 1120 °C are higher than those recorded for samples treated at 1180 °C. At the same heat treatment temperature, the fine microstructure (F) recorded lower corrosion rate values (95 and 21.5 mpy for 1120 F and 1180 F, respectively) compared with the coarse (C) microstructure (522 and 36 mpy for 1120 C and 1180 C, respectively). Based on the corrosion rate values of the four tested Ni-base alloys, Table 4, the sample with the coarse microstructure treated at 1120 ^oC recorded the highest corrosion rate, 522 mpy, (i.e., the lowest corrosion resistance) in 1.0 M H_2SO_4 solution, among the four tested Ni-base alloys.

Images of the optical microstructure of the blank sample, i.e., as polished, (image a) and the four tested samples after 96 h of immersion (images b-e), see Fig. 6, came to the same conclusion. It is seen that a general corrosion attack can be observed in all tested samples, as compared with the polished one (image a), which clearly shows the coarse primary tantalum carbides (TaC) in addition to the TCP phases. However, 1120 C and 1120 F exhibited the most severe attack, with intense corrosion clearly identifiable along the TCP phases. A less pronounced corrosion attack was observed on 1180 C, followed by 1180 F, which is easily comparable with the polished surface.

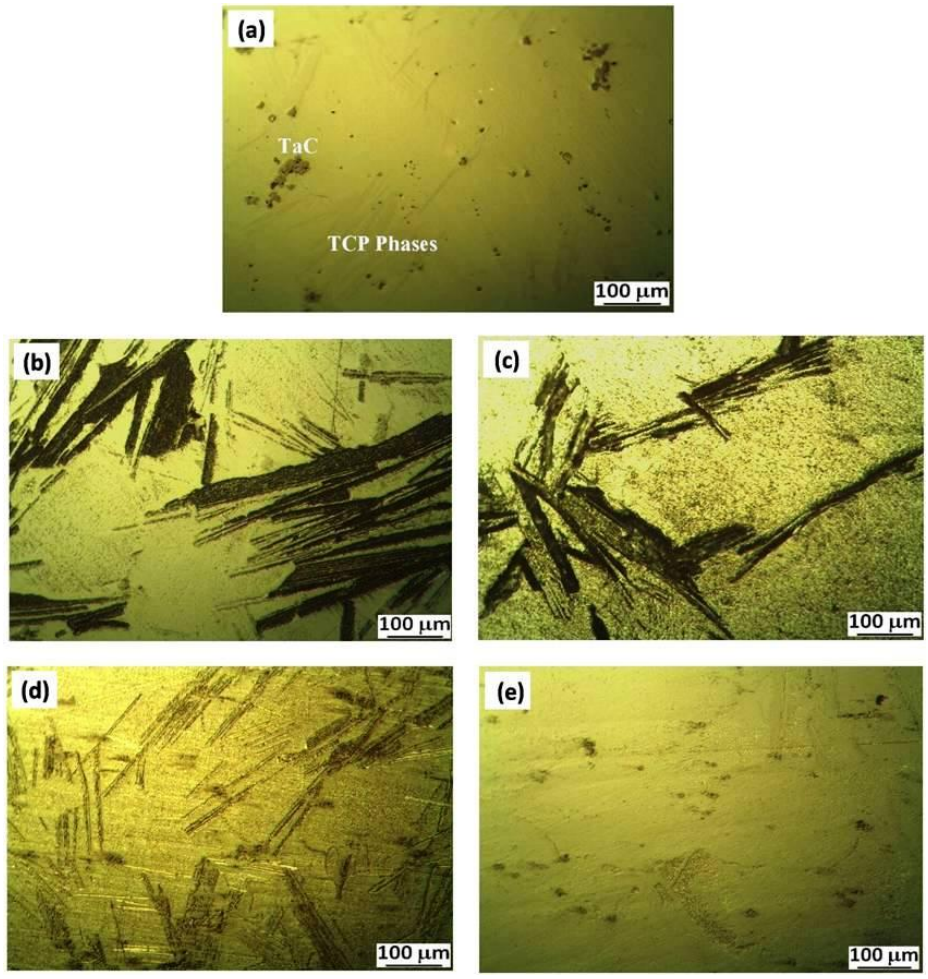

Figure 6. Optical microstructure recorded for **(a)** the blank sample, i.e., as polished, and the four tested samples after 96 h of immersion in 1.0 M H_2SO_4 solution at 25 ^oC, **(b)** sample 1120 C, **(c)** sample 1120 F, **(d)** sample 1180 C, **(e)** sample 1180 F.

This morphology could be attributed to the high corrosion rate promoted by the dissolution of TCP phases and Ni in the acid solution, and to the resulting strong cathodic reaction of hydrogen evolution. These results indicate that 1120 C and 1120 F alloys, under these conditions, are less corrosion resistant than 1180 C and 1180 F, and the corrosion resistance decreases with increase in TPC phases content in the tested sample. It seems therefore that the TCP phases exert a significant negative influence on the corrosion resistance of the tested Ni-base alloys in H_2SO_4 solutions to an extent depending on its content in the alloy, which in turn depends on the heat treatment conditions. The content of the TCP phases in the alloy is determined by the factor V_f, as previously discussed in sections 3.1 and 3.2.

Therefore, it will be much wiser to explain the corrosion behavior of these alloys adopting the effect of the heat treatment conditions on the microstructure of the tested samples, inspect again sections 3.1 and 3.2. It has been shown that higher temperature of solution treatment, 1180 °C, promotes dissolution of coarse γ' in the matrix much more than in case of low solution treatment temperature, 1120 °C, resulting in an obvious decrease in V_f of primary, coarse, γ'. This causes the

content of the TCP phases (the corrosion initiator) to decrease, thus corrosion rate obviously suppressed. This may explain why samples with low V_f values (see Table 2) are more corrosion resistant than samples with high V_f values (Table 4).

3.4.2. Potentiodynamic polarization measurements

Figure 7 presents the potentiodynamic polarization curves recorded for the tested alloys in 1.0 M H_2SO_4 solution at a scan rate of 2.0 mV s^{-1} at 25 ^oC.

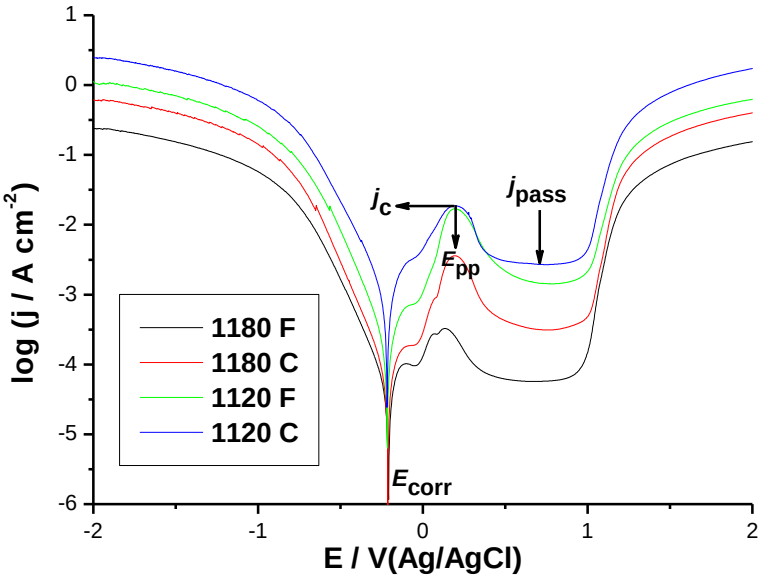

Figure 7. Potentiodynamic polarization curves recorded for the tested alloys in 1.0 M H_2SO_4 solution at a scan rate of 2.0 mV s^{-1} at 25 ^oC.

The cathodic branch of the polarization curve represents hydrogen evolution, while the anodic one shows alloy dissolution. The anodic domain can be divided into three regions; an active dissolution region, a region where there is a tendency of the alloy to passivate, and the third region in which the current density rises again with potential. In the anodic dissolution region, the kinetics of the anodic dissolution of the alloy may proceed via the reaction path presented in Eqs. 1-3. At more positive potentials, the current density decreases to an extent depending on the heat treatment conditions of the tested alloy. This decrease in anodic current may be attributed to the formation of the corrosion products and metal oxides on the alloy surface, which have some protective effect and reduce the active dissolution of metals from the surface (passivation). Further increase in potential causes the current to rise again, indicating that the formed passive films do not afford complete protection of the substrate alloy, and the alloy dissolution continues. Similar findings were previously

obtained by C.A. Della Rovere at al. [33] during studying the corrosion behavior of shape memory stainless steel in acid media.

It is obvious that the four tested alloys generally show similar active to passive transition behavior. The tested materials also showed the same transpassive breakdown potential. The corrosion potential (E_{corr}) values not significantly changed. Values of the cathodic Tafel slope (β_c) are almost the same. However, the anodic behavior of these materials was quite different in terms of the critical anodic current density required for passivation (j_c), the primary passive potential (E_{pp}), the passive current density (j_{pass}), and the extent of the passive region. Table 4 presents the different electrochemical parameters associated with polarization measurements for the tested alloys in 1.0 M H_2SO_4 solution at 25 ^oC. Some of these electrochemical parameters were derived from the polarization plots based on the Tafel extrapolation method, as shown in Fig. 8.

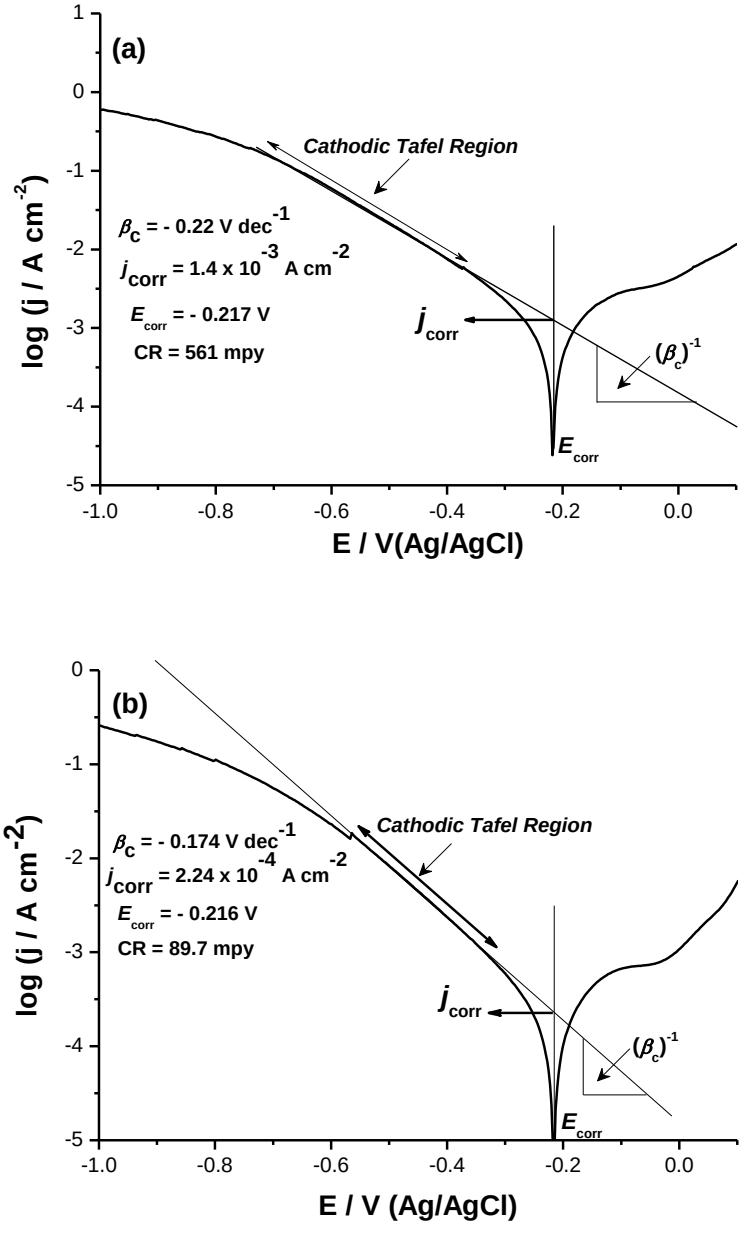

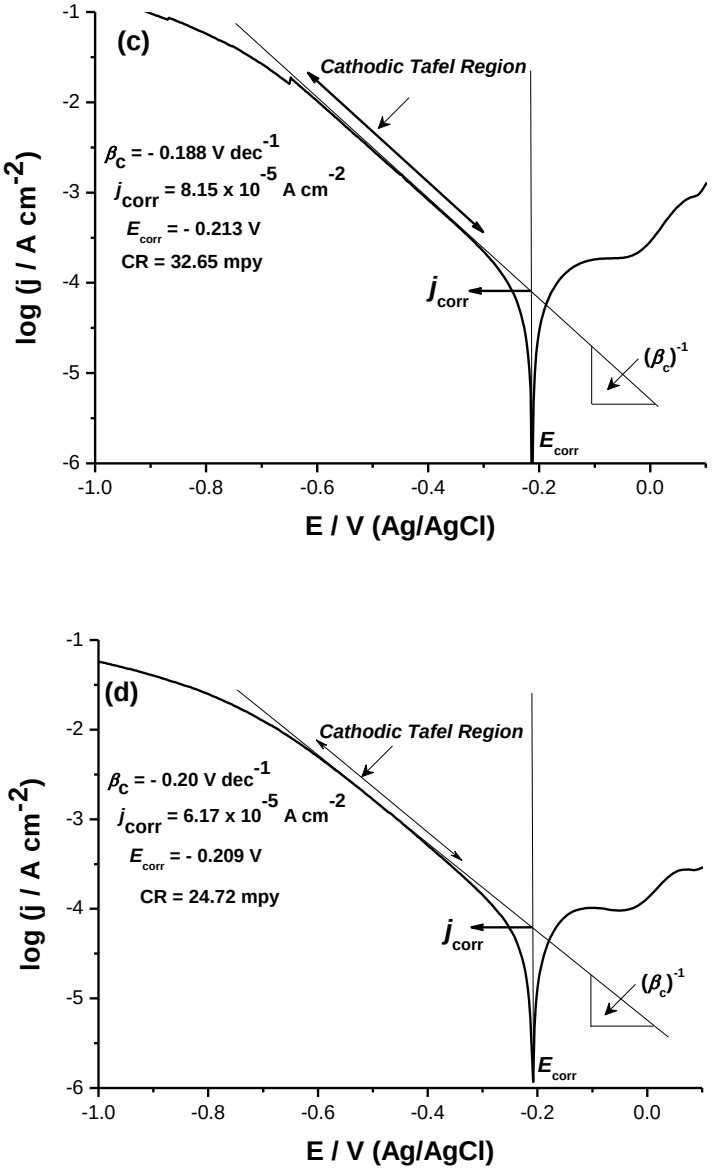

Figure 8. Calculations of some of the electrochemical parameters for the four tested Ni-base alloys in 1.0 M H_2SO_4 solution at a scan rate of 2.0 mV s^{-1} at 25 ^oC, based on Tafel extrapolation method, **(a)** 1120 C, **(b)** 1120 F, **(c)** 1180 C, **(d)** 1180 F.

Inspection of Table 4 reveals that the j_c and j_{pass} values of the samples treated at 1120 ^oC, namely and 1120 C and 1120 F, was found to be higher than those of samples treated at higher temperatures (1180 C and 1180 F). The high j_c and j_{pass} values of 1120 C and 1120 F indicate a greater difficulty to form protective passive film when compared to 1180 C and 1180 F. Based on the CR values evaluated from the Tafel extrapolation method (Table 4), the worst behavior was shown again by the sample 1120 C, which possesses the highest CR among the tested samples. It is interesting to note from Table 4 that the E_{pp} of the 1180 F alloy sample is more negative than that of the 1120 C sample, reflecting the higher tendency of the 1180 F sample to passivate. In addition, the 1180 F

sample recorded the least j_{pass} value (6 x 10^{-5} A cm^{-2}) among the tested alloys, indicating that the protectiveness and stability of the passive films formed on 1180 F is high compared with the other tested samples.

All these findings and events can be attributed, as previously discussed, to the higher values of V_f of the TCP phases of 1120 C and 1120 F compared with 1180 C and 1180 F (kindly inspect again V_f data presented in Table 2). The presence of TCP phases may accelerate corrosion and hinder the passivity of the tested alloy, resulting in higher j_c and j_{pass} values. As can be seen, the CR values obtained from the ICP method of chemical analysis are consistent with the CR values obtained from polarization measurements (Tafel extrapolation method for evaluation of corrosion rate). These results indicate that the corrosion rates determined by the polarization technique represent a good approximation of the real corrosion rates determined from the chemical tests. However, the advantage of the polarization technique is that it saves time.

4. CONCLUSION

Based on the results obtained regarding the effect of heat treatments on the microstructure and mechanical properties, as well as the corrosion behavior of Ni base superalloys in 1.0 M H_2SO_4 solution, the following conclusions can be drawn:

(i) The V_f of TCP phases in coarse microstructure (C specimen) is higher than that in case of fine structure (F specimen). Additionally, TCP phases are coarser in C specimens than in F ones.

(ii) Solution heat treatment at 1180 °C is more effective than solution treatment at 1120 °C in dissolving TCP phases in the γ matrix for both F and C specimens.

(iii) V_f of TCP phases in aged specimens treated at 1180 °C is lower than that treated at 1120 °C.

(iv) Chemical and electrochemical tests showed that the corrosion rates of F and C specimens with solution treatment at 1120 °C are higher than the rates of corrosion recorded for samples treated at 1180 °C.

(v) Chemical and electrochemical tests also revealed that, at same heat treatment temperature, the fine microstructure (F) recorded lower corrosion rates compared with the coarse (C) microstructure.

(vi) Optical microstructure examinations of the corroded samples showed that a general corrosion attack occurred along the TCP phases to an extent depending on the conditions of the heat treatments of the tested samples.

(vii) The tested Ni-base superalloys exhibited similar passive region, but their anodic behavior in the active region of dissolution differed significantly.

ACKNOWLEDGMENT

The authors gratefully acknowledge Taif University (Hawaiya, Saudia Arabia) for the financial support of this project (No. 1072).

References

1. R.A. Mackay, M.V. Nathal, and D.D. Pearson, *Metall. Trans.* A 21 (1990), 381.
2. J.D. Nystorm, T.M. Pollock, W.H. Murphy, and A. Garg, *Metall. Mater. Trans*. A 28 (1997) 2443.
3. X Yu, Y. Yamabe-Mitarai, Y. Ro, and H. Harada, *Metall. Trans*. A. 31 (2000) 173.
4. W. Wen-Juan, H. Guang-Wei, and D. Bo, J. *Iron. Steel Res. Int*. 17 (2010) 64.
5. J.S. Tiley, G.B. Viswanathan, A. Shiveley, M. Tschopp, R. Srinivasan, R. Banerjee, and H.L. Fraser, *J. Micron*. 315 (2010) 641.
6. S.A. Sajjadi, S. Nategh, and R.I. Guthrie, *Mater. Sci. Eng*. A 325 (2002) 484.
7. M. Aghaie-Khafri and M. Hajjavady, *Mater. Sci. Eng* A 487 (2008) 388.
8. X.Z. Qin, J.T. Guo, C. Yuan, J.S. Hou, and H.Q. Ye, *Mater. Lett*. 62 (2008) 258.
9. G.E. Fuchs, Mater. Sci. Eng. A 300 (2001) 52.
10. J.L. Liu, T. Jin, X.F. Sun, H.R. Guan, and Z.Q. Hu, *Mater. Sci. Eng*. A. 527 (2010) 890.
11. A.D. Sequeira, H.A. Calderon, G. Kostorz, *Scripta Metallurgica Materialia* 30 (1994) 75.
12. T. Grosdidier, A. Hazotte, A. Simon, *Scripta Metallurgica Materialia* 30 (1994) 1257.
13. S. Kraft, I. Altenberger, H. Mughrabi, *Scripta Metallurgica Materialia* 32 (1995) 411.
14. Y. Y. Qiu, *Acta Materialia* 44 (1996) 4969.
15. G.E. Fuchs, *Mater. Sci. Eng*. A 300 (2001) 52.
16. G.E. Fuchs, *J. Mater. Eng. Perform*. 11 (2002) 1925.
17. J.R. Davis, ASM Specialty Handbook: Nickel, Cobalt, and Their Alloys, Materials Park, Ohio, 2000.
18. H.J. Jang, C.J. Park, H.S. Kwon, *Electrochim. Acta* 50 (2005) 3503.
19. G. Frankel, *J. Electrochem. Soc.* 145 (1998) 2186.
20. O.M. Magnussen, J. Scherer, B.M. Ocko, R.J. Behm, *J. Phys. Chem*. B 104 (2000) 1222.
21. N. Pineau, C. Minot, V. Maurice, P. Marcus, *Electrochem. Solid-State Lett*. 6 (2003) B47.
22. A.Bouzoubaa, B. Diawara, V. Maurice, C. Minot, P. Marcus, *Corros. Sci*. 51 (2009) 2174.
23. S. Singh, S. Basu, A.K. Poswal, R.B. Tokas, S.K. Ghosh, *Corros. Sci*. 51 (2009) 575.
24. Tirdad Nickchi, Akram Alfantazi, *Corros. Sci*., 52 (2010) 4035.
25. N. El-Bagoury, A. Nofal, *J. Mater. Sci. Eng*. A, 527 (2010) 7793.
26. M.T. Kim, S.Y. Chang, J.B. Won, *Mater. Sci. Eng*. A 441 (2006) 126.
27. N. El-Bagoury, M.A. Waly, A.A. Nofal, *Mater. Sci. Eng*. A, 487 (2008) 152.
28. N. El-Bagoury, Q. Mohsen, "Gamma Prime and TCP phases and Mechanical Properties of Thermally Exposed Ni Base Superalloy" *Journal of Phase Transition* (2011), DOI: 10.1080/01411594.2011.582379.
29. Nader EL-Bagoury, *Journal of Heat Treatment and Materials* 66 (2011) 3.
30. J.R. Vilche, A.J. Arvia, *Corros. Sci.*, 15 (1975) 419.
31. E. McCafferty, *Corros. Sci*. 47 (2005) 3202.
32. ASTM G 102 – 89 (Reapproved 1999), Standard Practice for Calculation of Corrosion Rates and Related Information from Electrochemical Measurements.
33. C.A. Della Rovere, J.H. Alano, J. Otubo, S.E. Kuri, *J. Alloys and Compds*., 509 (2011) 5376.